# Stereo Tracking and 3D Reconstruction of Underwater Pipes

Vinicius Cesar[1]
vmc@cin.ufpe.br
Bernardo Reis[1]
bfrs@cin.ufpe.br
Saulo Pessoa[1]
sap@cin.ufpe.br
Judith Kelner[1]
jk@cin.ufpe.br
Ismael Santos[2]
ismaelh@petrobras.com.br

[1] Informatics Center
Federal University of Pernambuco
Recife, Brazil

[2] CENPES
Petrobras,
Rio de Janeiro, Brazil

**Abstract**

Installing flexible oil pipes in deep underwater environments is a risky operation, which is currently monitored by manually comparing the geometric conditions to the simulated studies. In order to avoid this error-prone assessment, this paper proposes an algorithm to track and reconstruct the pipe medial axis using stereo cameras. By taking advantage of the scenario illumination and the pipe texture, it is possible to devise an energy maximization approach that efficiently tracks the pipe. The reconstruction technique is an enhancement over a state-of-the-art B-spline reconstruction algorithm, specializing it for plane curves. Experiments on synthetic and laboratory videos report a very low mean tracking and reconstruction errors, while there are strong evidences of the robustness on a real scenario.

## 1 Introduction

In offshore oil production, the connection of flexible pipes from ships to wellbores is a delicate and recurrent operation on the seabed [13]. During this operation, excessive tension may be propagated from the pipe to the connector causing damage to the equipment. In order to mitigate such risks, physical simulations estimate in advance a safe geometric configuration that minimizes the stress in the connector. However, the current way to ensure that the pipe achieved the simulated configuration is by visually comparing it with images captured by video cameras installed in a ROV (Remotely Operated Vehicle). Since this comparison is an intense manual task that does not take into account perspective and lens distortions of the cameras, it is time-consuming and error-prone.

In order to provide an automatic solution that handles the assessment of the geometric configuration of the pipe, this paper presents a novel algorithm that tracks and reconstructs



Pages 137.1-137.12
DOI: https://dx.doi.org/10.5244/C.29.137

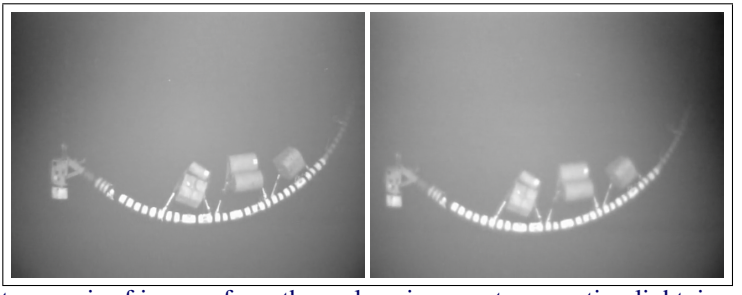

Figure 1: Stereo pair of images from the real environment, presenting lightning conditions, pipe marking, and auxiliary elements.

the Pipe Medial Axis (PMA). The proposed tracking algorithm consists of three steps: warping the pipe projection using its longitudinal and transversal parametrization; identifying the new longitudinal boundaries; and then maximizing the intensity of the pixels along the transversal dimension. Since the pipe is a deformable object, the 3D PMA is estimated using the state-of-the-art stereo curve reconstruction algorithm [18] on each stereo frame, which was adapted to impose a planarity constraint to the curve. The reconstructed curve plane is used in the following frame in order to evaluate the pipe projection. Our solution is evaluated in this paper on videos from synthetic and real scenarios, in which it achieves interactive rates. The experiments are based on tracking and reconstruction metrics, and proved that the algorithm is accurate and robust for practical aspects of the operation.

Detecting and tracking underwater pipes and cables are broadly investigated techniques for guiding autonomous underwater vehicles during maintenance and inspection procedures. However, they are commonly restricted to rigid pipes with small curvatures, allowing the pipe to be detected by using line extractors such as the Hough transform. In such scenario, [2, 14, 19] use similar approaches: preprocesses the image, segments it, extracts its contours, and then detects the pair of quasi-parallel lines that represent the borders of the pipe. Based on these lines, it is possible to estimate the position of the camera in relation to the pipe. In [6], the authors use morphological operations to extract the image contours as subjective uncertainties, which become input to a fuzzy inference system. The inference system detects the pipe position and generates the steering command for autonomous navigation. In order to track the pipe along the video, [15] temporally defines a region of interest to minimize the search space and follow the pipe using a Kalman Filter. Such approaches are not sufficient to solve the problem, since this scenario is specifically composed of flexible pipes.

## 2 Scenario

The connection operations take place in a deep underwater environment where sunlight is absent. Therefore, in order to visualize the pipe from a regular operation distance (about 15 m), it is necessary to utilize both underwater lamps and low-light underwater cameras. In spite of this imaging setup being usual in the offshore scenario, it can only produce monochrome and low-resolution images (RS-170 video standard) featuring a moderate amount of undesirable artifacts such as floating particles and tiny fish. Since this paper proposes a stereo system, two cameras in a parallel setup (80 cm apart from each other) are utilized.

Regarding the pipe, it is marked with an alternating pattern of contrasting colors. The purpose of this pattern is to provide longitudinal disambiguation texture. The algorithm also

takes advantage of the image background being darker than the pipe, something that naturally occurs due to the low-light condition. Finally, there is one more characteristic from which the algorithm benefits. Since a pipe installation operation takes place by hanging the pipe by its ends (one end is hanged by a crane whilst the other one remains attached to the boat), the pipe is compelled to configure a plane curve. However, there are auxiliary elements attached to the pipe, such as buoys and slings, that may compromise its tracking. Figure 1 shows an image sample from the stereo setup in the real environment.

## 3 Pipe Tracking

Aiming at the creation of a reliable reconstruction, the tracking algorithm must identify precisely the image of the PMA. In order to do that, the algorithm makes use of a priori information, such as the shape of the pipe and its radius. The pipe's radius is considered to be constant throughout its length. Regarding its shape, during the installation, it takes the shape of a curved string. Therefore, one can assume that the projection of a pipe onto the image describes a bi-dimensional curved region $\mathcal{R}$ of equation $\mathbf{R}(s,t;\mathbf{x}(t))$. The parameters $s$ and $t$ identify each pixel of the region and the $\mathbf{x}(t)$ is the projection of the PMA, which governs the region.

Due to the illumination characteristics of the scenario, where the background is darker than the foreground, one can also state that brighter pixels are more likely to belong to the pipe. Based on this hypothesis, the problem may be summarized as finding the curve that maximizes the intensity of the pipe projection pixels in the image $I$, i.e. maximizing the energy inside $\mathcal{R}$, as presented in Eq. 1:

$$\mathbf{x}^* = \arg\max_{\hat{\mathbf{x}}} \iint I(\mathbf{R}(s,t;\hat{\mathbf{x}}(t)))\,ds\,dt. \tag{1}$$

However, it is necessary to define the extremes of the pipe in the longitudinal direction in advance, otherwise maximizing Eq. 1 incurs in errors, such as a sudden collapse into a point or severe degeneration of the extremes. To solve this problem, the technique was divided into two unidimensional tracking phases. The first one locates the segment of the pipe along the longitudinal axis using the pattern marked over the pipe. The second one locates the pipe along the transversal direction of the PMA, applying Eq. 1.

A pipe might be thought of as a generalized cylinder whose medial axis is a segment of a parametric curve $\mathbf{X}(t)$ in 3D space, in which the pipe is defined in the interval $[t_{min}, t_{max}]$. Its surface is given by circumferences centered at and normal to each point of the medial axis. This way, each circumference is an infinitesimally thin transversal section of the pipe. Projecting every circumference onto the image forms the region $\mathcal{R}$, which can be parametrized by $t$ in the longitudinal direction (defined in the interval $[t_{min}, t_{max}]$) and $s$ in the transversal direction (defined in the interval $[0,1]$). The longitudinal parameter $t$ is the same of the curve $\mathbf{X}(t)$ and its projection $\mathbf{x}(t)$.

$\mathcal{R}$ is limited from above and from below by the curves $\mathbf{x}^+(t)$ and $\mathbf{x}^-(t)$, as illustrated in Figure 2a. These curves are the projection of rays that are tangential to the pipe at the 3D curves $\mathbf{X}^+(t)$ and $\mathbf{X}^-(t)$, as illustrated in Figure 2b. Thus, $\mathcal{R}$ is defined by the equation $\mathbf{R}(s,t) = (1-s)\,\mathbf{x}^-(t) + s\,\mathbf{x}^+(t)$, where the curve $\mathbf{x}(t)$ is omitted from the arguments of $\mathbf{R}$ for the sake of clarity. Observe that parameter $s$ in $\mathbf{R}(s,t)$ varies over a line from $\mathbf{x}^+(t)$ to $\mathbf{x}^-(t)$, and not over the projection of a circumference. While significantly faster to calculate, the linear traversal has shown similar results in synthetic experiments. Through this model it is

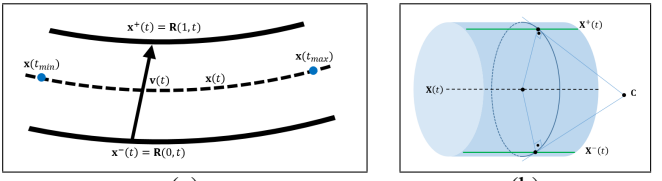


(a) (b)

Figure 2: Parametrization of $\mathcal{R}$ (a) based on the pipe tangential curves $\mathbf{X}^+$ and $\mathbf{X}^-$ (b)

possible to rectify the pipe projection into a rectangular box, assisting the tracking technique. This transform is explained in the following section.

## 3.1 Image Transform

The first step of the proposed technique is to transform the input image from the spatial domain to the longitudinal and transversal parametrization based on the curve. This procedure aims at simplifying the tracking technique, and consequently accelerating its execution. The transform is defined as

$$T(s,u) = \sqrt{I(\mathbf{R}(s,t))}, \quad \text{where } u = \int_{t_{min}}^{t} \left|\left| \frac{d\mathbf{x}(\tau)}{d\tau} \right|\right| d\tau. \tag{2}$$

The parametrization of $u$ as the arch length was chosen to guarantee that the curve keeps its length after the transformation. It is defined in the interval $[u_{min}, u_{max}]$. This transform creates significant distortions in parts of the image far from the curve, so it is recommended to apply it only to the neighborhood of the curve. However, it is necessary to find the pipe in the current frame, which has moved a little from its position in the previous frame. In order to still encompass the pipe in the transform, the interval of the parameters $u$ and $s$ is extrapolated from the previous frame by $\delta_s$ and $\delta_u$, such that the transformed image is defined in the interval $-\delta_s \leq s \leq 1+\delta_s$ and $u_{min} - \delta_u \leq u \leq u_{max} + \delta_u$. This extrapolation is generally small, since both the pipe and the camera are subject only to slow movements. A transformed image example is given in Figure 6f.

Several benefits arise from using this transform, such as avoiding to repeatedly evaluate both $\mathbf{R}(s,t)$ and the square root operation during the tracking. The transformed image is also smaller than the original one, accelerating the filtering steps. And the transversal and longitudinal tracking become simpler, since they act in the horizontal and vertical direction of the transformed image $T$, as explained below.

## 3.2 Tracking Approach

The adopted strategy to solve the tracking problem consists in splitting it into two phases: the longitudinal tracking, which identifies the new position of the extremes of the pipe segment in the longitudinal direction; and the transversal tracking, which adjusts the whole curve in the transversal direction.

### 3.2.1 Longitudinal Tracking

Given the projection of a curve that has moved slightly from the previous frame, the longitudinal tracking seeks to define a new interval $[u^*_{min}, u^*_{max}]$ in the $u$ direction where the curve

is found in the current frame. The algorithm takes advantage of the pattern marked over the pipe to guarantee that the same pipe segment is being tracked along the time. Since the pattern is composed of a bright region followed by a dark region, it is established that the pipe's extremities lay upon a brighter region. Therefore, the tracking is done by maximizing the energy in a window around the pipe extremity along the $u$ direction, using a Gauss-Newton approach, such that

$$u^* = \arg\max_{\hat{u}} \int_{\hat{u}-\omega/2}^{\hat{u}+\omega/2} \int_0^1 T(s,u)^2 \, ds \, du \tag{3}$$

The window is defined by the interval $0 \leq s \leq 1$ in the transversal direction, and $u_{min} - \omega/2 \leq u \leq u_{min} + \omega/2$ in the longitudinal direction for the left extremity, and $u_{max} - \omega/2 \leq u \leq u_{max} + \omega/2$ for the right extremity. The $\omega$ defines the window width and has been empirically evaluated to be as large as the thickness of the pipe projection, which is considered to be constant between two frames, but is updated at the end of the reconstruction. Each extremity is tracked separately, so that an approach or a retreat is correctly handled.

### 3.2.2 Transversal Tracking

As the projection of the pipe generally has brighter pixels than the background, the transversal tracking aims to maximize the energy inside the transformed image $T(s,u)$ of the region $\mathcal{R}$ along the $s$ dimension, once the longitudinal tracking has already identified the position of the new extremes of the pipe along the $u$ dimension. This is done by adjusting the previously detected medial axis by a smooth function $\phi(u;\mathbf{q})$, which is governed by the parameter vector $\mathbf{q}$ and $u$ defined in the interval $[u^*_{min}, u^*_{max}]$. This way, Eq. 1 is updated and the problem described as finding the parameter vector $\mathbf{q}^*$, such that

$$\mathbf{q}^* = \arg\max_{\hat{\mathbf{q}}} \int_0^1 \int_{u^*_{min}}^{u^*_{max}} w(s) \; T(s + \phi(u;\hat{\mathbf{q}}), u)^2 \, du \, ds, \tag{4}$$

where $w(s)$ is a weighting function defined as $w(s) = \min[s/\alpha, 1, (1-s)/\alpha]$, $0 < \alpha \leq 1$. The weighting function is used to increase the robustness of the tracking around the border of the pipe. Since accessories on the pipe, parts with smaller or greater diameter, and failure in the pipe markings might tamper with the border of the pipe in the image, this region has a lower weight than the center region, which is generally more well-behaved. The $\alpha$ parameter defines how much of boundary must be considered border and the value 0.2 was perceived to give accurate results.

The function (4) can be maximized by transforming it in a least-square problem. Given that the pipe accounts for $m \times n$ pixels in the discretizaton of the transformed image $T$, one may rewrite the function (4) as

$$\sum_{i=0}^{n-1} \sum_{j=0}^{m-1} \left( \sqrt{w(s_j)} \; T\left(s_j + \phi(u_i;\mathbf{q}), u_i\right) \right)^2, \tag{5}$$

which can be maximized using a Gauss-Newton method.

In order to provide smoothness to the tracking, a good option to model the function $\phi(u)$ is the B-splines, which are parametric smooth piecewise polynomial functions governed by control points. Each point given by $\phi(u)$ is an average of the control points weighted by a basis function $N^i(u)$. Thus, given $\gamma$ unidimensional points $\mathbf{q} = [q_0, ..., q_{\gamma-1}]^\top$, the function $\phi(u;\mathbf{q}) = \sum_i N^i(u) \, q_i = \mathbf{N}(u)^\top \mathbf{q}$, where $\mathbf{N} : \mathbb{R} \to \mathbb{R}^\gamma$ is a vectorial function.

In the Gauss-Newton method, the step is calculated as $\Delta\mathbf{q} = (\mathsf{J}^\top\mathsf{J})^{-1}\mathsf{J}^\top\mathbf{r}$, where $\mathsf{J}$ is the Jacobian of Eq. 5 and $\mathbf{r}$ is the residual vector. Using the chain rule to determine the derivative of Eq. 5, one obtains $\mathbf{J}_{(i,j)} = \mathbf{N}(u_i)T_s^{(i,j)}$, where $\mathbf{J}_{(i,j)}$ is the $(m \times i + j)^{\text{th}}$ row of $\mathsf{J}$. Since $\mathbf{N}(u_i)$ may be precomputed, it results in the following simplification.

$$\mathsf{J}^\top\mathsf{J} = \sum_i \sum_j \mathbf{N}(u_i)\mathbf{N}(u_i)^\top w(s_j)(T_s^{(i,j)})^2 = \sum_i \mathbf{N}(u_i)\mathbf{N}(u_i)^\top \sum_j w(s_j)(T_s^{(i,j)})^2, \tag{6}$$

where, for the sake of clarity, $T^{(i,j)} = T(s_j + \phi(u_i;\mathbf{q}), u_i)$ and $T_s^{(i,j)}$ is the derivative of the pixel $T^{(i,j)}$ in $s$ direction. In a similar way

$$\mathsf{J}^\top\mathbf{r} = \sum_i \sum_j \mathbf{N}(u_i)w(s_j)T_s^{(i,j)}T^{(i,j)} = \sum_i \mathbf{N}(u_i)\sum_j w(s_j)T_s^{(i,j)}T^{(i,j)}. \tag{7}$$

Naively computing $\mathsf{J}^\top\mathsf{J}$ has a cost of $m \times n \times \gamma^2$, which is time-consuming to do iteratively. On the other hand, by using Eq. 6, it will cost only $m \times (n + \gamma^2)$. On top of that, only non-zero elements of $\mathsf{J}^\top\mathsf{J}$ need to be computed. These simplifications speed up the computation by one order of magnitude. Considering that the displacement of $\mathbf{x}(t)$ is equivalent to those of $\mathbf{x}^+(t)$ and $\mathbf{x}^-(t)$, the curve is updated by $\mathbf{x}^*(t) = \mathbf{x}(t) + \phi(t;\mathbf{q}^*)\mathbf{v}(t)$, where $\mathbf{v}(t) = \mathbf{x}^+(t) - \mathbf{x}^-(t)$ is a vector in the transversal direction.

This solution has been described so far in a continuous approach, but, in practice, the input for the reconstruction algorithm is a set of points of the curve $\mathbf{x}^*(t)$. In order to obtain a suitable discretization, the curve derivatives can be estimated using a B-spline approximation to compute $\mathbf{x}^+(t)$ and $\mathbf{x}^-(t)$ in discrete form.

## 4 Stereo Reconstruction of Plane Curves

Given the output of the tracking algorithm — two sets of sample points $\{\mathbf{p}_i\}$ and $\{\mathbf{p}'_j\}$, regarding the left and right images, respectively — the stereo reconstruction objective is to estimate the PMA, i.e. the 3D curve $\mathbf{X}(t)$. Reconstruction of primitives such as conics, splines, and algebraic curves has already been investigated in [1, 5, 6, 7, 10, 16, 18]. Among the possibilities, the most appropriate was considered that of modeling the PMA as a B-spline, due to its generality and the feasibility to apply bundle adjustment [17] as a means to find the optimal reconstruction, as Yi Xiao and Y. Li mentioned in [18].

Yi Xiao and Y. Li showed that, in order to reconstruct rational B-spline curves, it is necessary to simultaneously fit a rational B-spline to each of the sample points $\{\mathbf{p}_i\}$ and $\{\mathbf{p}'_j\}$. It results in the curves $\mathbf{x}(t;\{\mathbf{q}_k\})$ on the left image and $\mathbf{x}(t;\{\mathbf{q}'_k\})$ on the right image, where $\{\mathbf{q}_k\} = \{[q_x^k, q_y^k, q_w^k]^\top\}$ and $\{\mathbf{q}'_k\} = \{[q_x'^k, q_y'^k, q_w'^k]^\top\}$ are the control points of the B-splines in homogeneous coordinates. This fitting can be modeled as a least-squares problem and solved minimizing the cost

$$\sum_i ||\mathbf{p}_i - \mathbf{x}(t_i;\{\mathbf{q}_k\})||^2 + \sum_j ||\mathbf{p}'_j - \mathbf{x}(t_j;\{\mathbf{q}'_k\})||^2, \tag{8}$$

where $t_i$ and $t_j$ are the sampling parameters of $\mathbf{p}_i$ and $\mathbf{p}'_j$ respectively. If the sample points are rectified, the epipolar constraint imposes that the vertical coordinates are equal when solving Eq. 8, i.e. $q_y^k = \mu\, q_y'^k$ and $q_w^k = \mu\, q_w'^k$, for any non-zero constant $\mu$. The control points of the reconstructed curve are obtained from $\{\mathbf{q}_k\}$ and $\{\mathbf{q}'_k\}$ as described in [18].

Our contribution is to add a new constraint to ensure that the reconstructed curve lies on a plane. This constraint implies that the curve projection in both cameras are related by a homography $\mathsf{H}$ [9], as well as $\{\mathbf{q}_k\}$ and $\{\mathbf{q}'_k\}$ [18]. Since the sample points are rectified, the homography $\mathsf{H}$ can alter only the $x$ coordinates of the curve points. Therefore, it becomes an affine transformation imposing the following constraints to the control points

$$q'^k_x = \mu(a\,q^k_x + b\,q^k_y + c), \quad q'^k_y = \mu\,q^k_y \quad \text{and} \quad q'^k_w = \mu\,q^k_w, \tag{9}$$

where $[a,b,c]^\top$ is the first row of $\mathsf{H}$.

The reconstruction problem is then solved using the Levenberg-Marquardt algorithm to minimize Eq. 8, given the constraints (9). The parameters $t_i$ and $t_j$ are not optimized because the projection of the pipe is a smooth curve. Instead, they are calculated using the centripetal parametrization [11], which defines the interval length between the parameters of two sequential points as $d_i = ||\mathbf{p}_{i+1} - \mathbf{p}_i||^{1/2}$, given that $t_{i+1} = t_i + d_i$ and $t_0 = 0$. The weights $q'^k_w$ and $q^k_w$ are set to 1, and consequently $2\gamma+3$ values are optimized in Eq. 8, where $\gamma$ is the number of control points: two parameters for each control point, and three parameters for the affinity $\mathsf{H}$ that maps the left curve to the right curve complying to Eq. 9.

Regarding the accuracy of the reconstructed curve, it has been found to be greatly influenced by the angle between the normal of the curve plane and the optical axis of the camera. This angle is denominated *obliquity*, and denoted as $\theta$ in Figure 3c. For the sake of simplicity, the analogous problem in 2D, the reconstruction of a line segment, will be considered. Due to the scenario characteristics, the distance from the pipe to the cameras tends to be much greater than the baseline, which makes the uncertainty of the reconstruction on $Z$ axis (depth) much greater than on $X$ axis, as illustrated in Figure 3a. As the obliquity grows, line segments increasingly stretched become a subset of the uncertainty region (in light blue in Figure 3b), which is estimated based on the uncertainty of each point of the segment. Considering the worst case of line segment reconstruction (dashed red line), the length error in Figure 3c is almost six times greater than that in Figure 3b due to the obliquity. This error also varies according to the ratio of the distance between the pipe and the camera over the length of the pipe segment. This stretching is reflected in the 3D plane curve.

# 5 Results

Videos from synthetic and real scenarios were used on the experiments (see supplementary material), both of them having $640 \times 480$ pixels of resolution. Two real scenarios were considered: one was constructed in laboratory; and the other is an actual offshore operation. For synthetic and laboratory scenarios, the ground-truth was known, since hand-made pipes on catenary [12] configurations were used. A catenary curve is defined by an *amplitude* parameter and expresses the curve formed by an uniformly dense, perfectly flexible, and inextensible cable hanged by its endpoints. Although real pipes do not configure such a catenary due to their natural bending resistance, it is a suitable curve model for the experiments.

The results presented in this section were generated on an Intel Core i7-4810MQ processor with 16 GB of RAM memory. The proposed algorithm was implemented sequentially in C++ and compiled with Microsoft Visual C++ 2012, using image processing routines from OpenCV library [4] and the Eigen library [8] for linear algebra operations. The tracking algorithm execution time depends on the number of iterations taken to converge the optimization in both phases, and on the area of the image belonging to the pipe. The total execution time

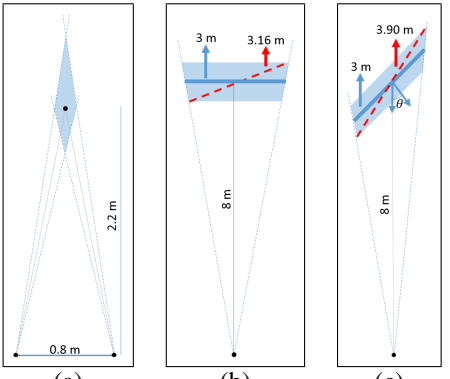


(a) (b) (c)

Figure 3: Uncertainty of the reconstruction of a point (a), non-oblique (b) and oblique (c) plane.

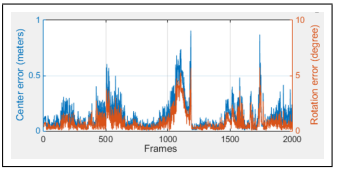


(a)

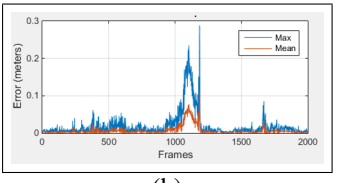


(b)

Figure 4: Error of the camera poses (a) and the reconstruction error (b).

for each image averaged $10 \pm 3$ ms. Likewise, the reconstruction algorithm execution time depends on the number of iterations and the length of the PMA. It averaged 6 ms on clear images, and 12 ms on turbid images. This increase is due to a non-smooth projection of the PMA, which increased the number of iterations.

## 5.1 Synthetic Videos

The synthetic scenario was created based on a real offshore one: cameras with 90° of horizontal FOV were placed 80 cm apart from each other; and a 40 cm diameter pipe, configured such as a 4 m amplitude catenary, was modeled and textured with alternating contrasting colors. A video sequence with 2000 frames exploring multiple camera viewpoints (near, far, and oblique) was rendered. Since this scenario is not subject to camera calibration errors and noise, a precise evaluation of the influence of the obliquity can be performed.

The tracked curve is assessed by the *tracking error* metric — the distance between the tracked points and the projection of the ground-truth catenary in pixels. The mean of the tracking error was $0.011 \pm 0.03$ pixels, the maximum error was 0.646 pixels, and the error was less than 0.1 pixel in 98.20% of the tracked points. The most significant error occurred in the curve's ends due to jittering of the longitudinal tracking while it expands.

Odometry errors were measured assuming that the pipe is static (Figure 4a). In such case, the camera center error averaged 0.1249 m and the rotation error, 0.79°. The *reconstruction error* — the distance between the tracked points and the ground-truth catenary in meters — was also measured resulting in a mean error of 0.0066 m (Figure 4b). In summary, even though the synthetic video sequence is free of noise, the cameras' position was not precisely recovered. However, the geometry of the PMA (the most valuable information) was measured with an inconsequential error. A fact worth remarking is that the worst results were achieved around frames 500, 1100, and 1700, exactly where there is more obliquity.

## 5.2 Real Videos

A pair of properly calibrated Kongsberg OE15-101c cameras were used on the tests at the real scenario. By using an iron chain wrapped with soft foam, a shape similar to a pipe with

| Video | L1 | L2 | L3 | L4 | L5 | L6 | L7 | L8 |
|---|---|---|---|---|---|---|---|---|
| Amplitude | 44.75 | 31.20 | 25.04 | 61.57 | 29.95 | 54.69 | 29.95 | 54.69 |
| Mean | 0.37 | 0.35 | 0.71 | 0.30 | 0.24 | 0.13 | 0.61 | 0.26 |
| Std | 0.12 | 0.20 | 0.40 | 0.18 | 0.11 | 0.07 | 0.35 | 0.15 |
| Max | 0.85 | 1.00 | 1.72 | 0.83 | 0.60 | 0.38 | 1.33 | 0.65 |

Table 1: Reconstruction error in centimeters of laboratory videos.

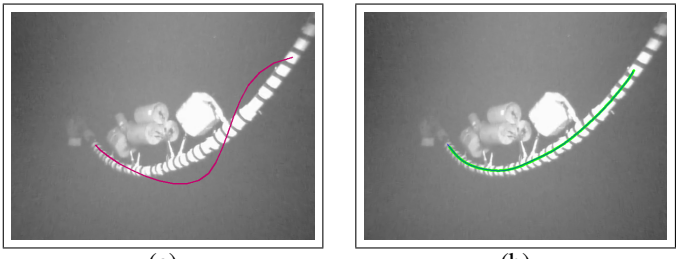

(a) (b)

Figure 5: Tracking robustness to poor initialization. (a) shows in magenta the initialization, and (b) presents in green the tracked curve at the following frame.

5.6 cm of diameter was created, in a scale of 1 : 8.89. When suspended it shapes itself as a catenary, whose amplitude was manually measured before each test to be used as ground-truth. The cameras were positioned 9 cm apart from each other and the pipe's distance to the cameras was between 1 m and 2.5 m.

The laboratory videos explored oblique viewpoints from different distances. Table 1 summarizes the results. The mean reconstruction error was less than 0.5 cm in 7 of 8 videos and the deviation was small, demonstrating stability. The maximum error was 1.72 cm (a third of the pipe's diameter) and occurred in the curve's ends. Despite the curve being unstable during video L2 due to water turbidity, the technique presented a precise reconstruction.

The algorithm was also evaluated in videos of real operations, where the cameras were placed 80 cm apart from each other. Objects attached to the pipe, such as the buoys and slings, disturbed the tracked curve. Nevertheless, the technique is quite robust to poor initialization, being able to recover from an initialization even with input points placed outside of the pipe projection, such as presented in Figure 5. The smooth function attenuates the effect from the attached objects (Figure 6a). Figure 6b presents the proposed technique correctly tracking a pipe with non-uniform diameter. Figure 6c shows frames of an approach that was stably tracked and expanded (video R4 in supplementary material). The pipe plane is correctly estimated, given the correct thickness of the pipe projection region.

The proposed algorithm can track pipes even in low-light and noisy images (Figure 6d and video R1 in supplementary material), although with some instability. Oblique cases are also properly tracked, such as the one depicted in Figure 6e (the warped image is shown in 6f) (video R2 in supplementary material). This latter scenario was assessed by comparing the plane of the reconstructed curve with a plane estimated from sonar data. The plane estimated from sonar data has obliquity equal to 46.29°, and the angle between the normal of the reconstructed plane and the plane estimated by the sonar is only 0.5°. The point of the curve directly in front of the ROV has its distance estimated by the sonar in 11.56 m, while this same point is estimated by our technique in 11.66 m. In addition, since the tracking results are visually correct in the images, a precise reconstruction of the curve is supposed.

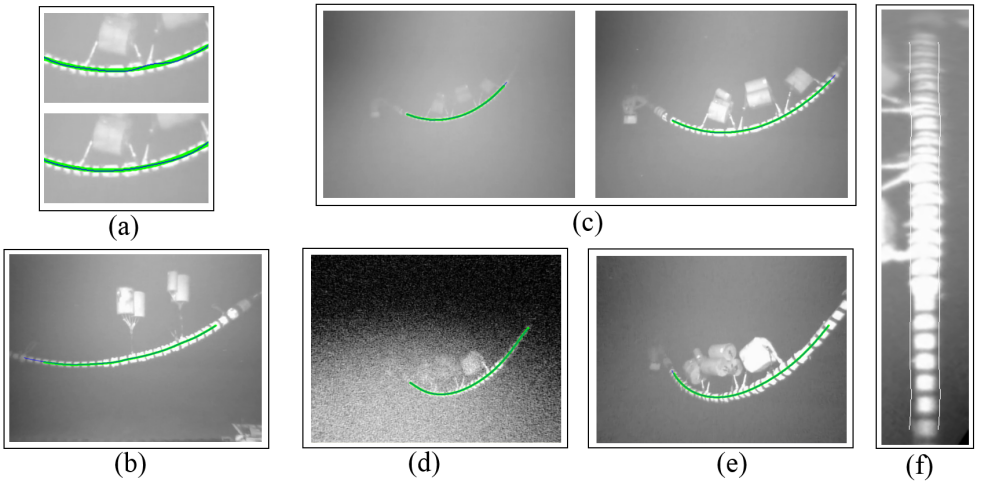


Figure 6: Sample frames of real videos: (a) shows smoothness improvement provided by the weighting function. (b)-(e) depict tracking results in diverse circumstances. (f) is the warped image of (e). The blue line represents the tracked curve and the green curve is the projection of the reconstructed curve onto the image.

# 6 Conclusions

The experiments show that the proposed technique is stable, accurate, and robust for evaluating the geometry of the pipe in standard operation arrangements. However, jitter was observed in the sections of the curve closer to its extremities, since the pixels beyond it are not considered during the expansion on the longitudinal tracking. This causes the maximum reconstruction error to be high on these sections. On adverse situations, such as fast movements and the absence of features, the tracking algorithm failed to follow the pipe in the image. Furthermore, on arrangements with high obliquity, the reconstruction error increases.

Regarding the experiments on the real scenario, the accurate plane reconstruction, even under high obliquity, is an evidence of the correct reconstruction of the PMA. This evidence is strong, given the laboratory accurate reconstruction results. The technique is also fast, taking the mean time per frame of 29 ms, including both tracking and reconstruction. The tracking running time is proportional to the area of the pipe projection onto the image. In future works, it is worth evaluating the adherence of the reconstructed curve to the simulated one. While this paper only explores the technique in the context of underwater pipes, the proposed stratified tracking using B-splines should be useful for different deformable objects, such as belts, chains, wires and cords.

**Acknowledgements:** This research was supported by Petrobras and FINEP (TRACKPETRO project). Vinicius Cesar would like to thank CNPq for his master's scholarship, and Saulo Pessoa would like to thank FACEPE for his PhD scholarship.

# References


[1] MH An and CN Lee. Stereo vision based on algebraic curves. In *Pattern Recognition, 1996., Proceedings of the 13th International Conference on*, volume 1, pages 476–482. IEEE, 1996.

[2] Muhammad Asif and Mohd Rizal Arshad. *An active contour and kalman filter for underwater target tracking and navigation*. INTECH Open Access Publisher, 2006.

[3] Rikard Berthilsson, Kalle Åström, and Anders Heyden. Reconstruction of general curves, using factorization and bundle adjustment. *International Journal of Computer Vision*, 41(3):171–182, 2001.

[4] G. Bradski. Opencv. *Dr. Dobb's Journal of Software Tools*, 2000.

[5] Kia Chua and Mohd Rizal. Robotics vision-based heuristic reasoning for underwater target tracking and navigation. In *Mobile Robots: towards New Applications*. InTech, dec 2006. doi: 10.5772/4700. URL http://dx.doi.org/10.5772/4700.

[6] Song De Ma. Conics-based stereo, motion estimation, and pose determination. *International journal of computer vision*, 10(1):7–25, 1993.

[7] Olivier Faugeras and Théo Papadopoulo. A theory of the motion fields of curves. *International Journal of Computer Vision*, 10(2):125–156, 1993.

[8] Gaël Guennebaud, Benoît Jacob, et al. Eigen v3. http://eigen.tuxfamily.org, 2010.

[9] Richard Hartley and Andrew Zisserman. *Multiple view geometry in computer vision*. Cambridge university press, 2003.

[10] Jeremy Yermiyahou Kaminski, Michael Fryers, Amnon Shashua, and Mina Teicher. Multiple view geometry of non-planar algebraic curves. In *Computer Vision, 2001. ICCV 2001. Proceedings. Eighth IEEE International Conference on*, volume 2, pages 181–186. IEEE, 2001.

[11] E.T.Y. Lee. Choosing nodes in parametric curve interpolation. *Computer-Aided Design*, 21(6):363 – 370, 1989. ISSN 0010-4485. doi: http://dx.doi.org/10.1016/0010-4485(89)90003-1. URL http://www.sciencedirect.com/science/article/pii/0010448589900031.

[12] Edward Harrington Lockwood. *A book of curves*. Cambridge University Press, 1971.

[13] FJM Nagle, JE Mendonça da Silva, LA Costa, and RW Capllonch. Vertical connection system for flexible pipes: Offshore tests and pioneer installation. In *Offshore Technology Conference*, 1993.

[14] M. Narimani, S. Nazem, and M. Loueipour. Robotics vision-based system for an underwater pipeline and cable tracker. In *OCEANS 2009 - EUROPE*, pages 1–6, May 2009. doi: 10.1109/OCEANSE.2009.5278327.

[15] Alberto Ortiz, Miquel Simó, and Gabriel Oliver. A vision system for an underwater cable tracker. *Machine vision and applications*, 13(3):129–140, 2002.

[16] Long Quan. Conic reconstruction and correspondence from two views. *Pattern Analysis and Machine Intelligence, IEEE Transactions on*, 18(2):151–160, 1996.

[17] Bill Triggs, Philip F McLauchlan, Richard I Hartley, and Andrew W Fitzgibbon. Bundle adjustment - a modern synthesis. In *Vision algorithms: theory and practice*, pages 298–372. Springer, 2000.

[18] Yi Jun Xiao and YF Li. Optimized stereo reconstruction of free-form space curves based on a nonuniform rational b-spline model. *JOSA A*, 22(9):1746–1762, 2005.

[19] Tie-dong Zhang, Wen-jing Zeng, Lei Wan, and Zai-bai Qin. Vision-based system of auv for an underwater pipeline tracker. *China Ocean Engineering*, 26(3):547–554, 2012. ISSN 0890-5487. doi: 10.1007/s13344-012-0041-1. URL http://dx.doi.org/10.1007/s13344-012-0041-1.